Hydrophobic Interaction and Charge Accumulation at the Diamond-Electrolyte Interface

M. Dankerl, A. Lippert, S. Birner, E. U. Stützel, M. Stutzmann, and J. A. Garrido*

Walter Schottky Institut, Technische Universität München, Am Coulombwall 4, 85748 Garching, Germany

(Received 9 February 2011; published 13 May 2011)

The hydrophobic interaction of surfaces with water is a well-known phenomenon, but experimental evidence of its influence on biosensor devices has been lacking. In this work we investigate diamond field-effect devices, reporting on Hall effect experiments and complementary simulations of the interfacial potential at the hydrogen-terminated diamond/aqueous electrolyte interface. The interfacial capacitance, derived from the gate-dependent Hall carrier concentration, can be modeled only when considering the hydrophobic nature of this surface and its influence on the structure of interfacial water. Our work demonstrates how profoundly the performance of potentiometric biosensor devices can be affected by their surfaces' hydrophobicity.

DOI: 10.1103/PhysRevLett.106.196103 PACS numbers: 68.08.De, 73.40.Mr, 81.05.ug

Interfaces with water play a decisive role in biosensors and bioelectronic devices, whose potential applications have so far barely been realized. The leading role of silicon in these fields is being challenged by materials such as diamond, graphene, and carbon nanotubes, precisely because of a more suitable set of interfacial properties, in particular, a better stability in electrolytes [1–3]. The diamond/aqueous electrolyte interface, for example, has been shown to be a successful platform for biosensor as well as for bioelectronic applications due to its chemical and electrochemical stability, biocompatibility, and functionalization possibilities [4,5]. Furthermore, these carbon-based materials offer an additional distinct feature: Their surface can be made strongly hydrophobic. In this context, it is particularly relevant to recognize that the hydrophobicity of a surface has a major effect on its interaction with water. It has been shown, for instance, that hydrophobicity leads to a depletion of water in the vicinity of the surface [6]. To date, however, the effect of this surface property has barely been considered to explain the operation of, e.g., biosensor devices. The hydrophilic nature of the more commonly employed oxide surfaces hides any relevant effect of the hydrophobicity-driven water depletion. However, since many of the highly promising materials for these applications such as diamond, graphene, or organic semiconductors exhibit strong hydrophobicity, this effect can no longer be ignored when considering the operation of such devices. In many biosensors and bioelectronic devices, potential changes across their interface with water modulate the concentration of charge carriers, and consequently the conductivity, leading to the sensor signals. This potential-dependent charge in the conductive channel found, e.g., in field-effect transistors, constitutes the capacitance of the interface, analogous to a plate capacitor. For the case of hydrophobic materials, water depletion close to the surface is bound to have an impact on the capacitance, as it will modify the dielectric constant close to the surface as well as determine how far the charge carriers on the water side (ions) are separated from the surface. In Si/SiO_2-based field-effect transistor devices such an effect is negligible, not only due to their hydrophilic nature but also because the oxide acts as a dielectric spacer between the charges in the semiconductor and the water, thus masking the effect of an additional hydrophobic separation.

In this work, we use surface-conductive diamond as a model hydrophobic material. With a band gap of 5.45 eV, intrinsic diamond is an insulator. However, the termination of the diamond surface with hydrogen renders the surface hydrophobic and results in a negative electron affinity χ of about -1 eV, which causes a p-type surface conductivity of hydrogen-terminated diamond [7,8]. The electrochemical stability of the diamond surface allows the insertion of this material into an electrolyte solution and the application of potentials between the electrically contacted diamond surface and a reference electrode in the electrolyte. The potential across the hydrogen-terminated diamond/aqueous electrolyte interface determines the position of the Fermi level at the diamond surface. If the Fermi level is pushed below the valence band edge, holes can be accumulated in a two-dimensional hole gas, whereby the position of the Fermi level determines the number of carriers [see Fig. 1(a)] [9–11]. According to this description, the hole concentration in the diamond increases with the applied voltage, where the capacitance of the interface determines the respective part of the voltage drop in the diamond and in the electrolyte. Here, we investigate the carrier accumulation at the hydrophobic surface of hydrogen-terminated diamond, at the interface to an aqueous electrolyte employing in-liquid Hall effect measurements. Furthermore, the potential distribution across the interface and the resulting charge accumulation are modeled by using an extended Poisson-Boltzmann distribution for ions in the electrolyte, which considers a spatially varying dielectric constant and the potential of mean force for the electrolyte ions.

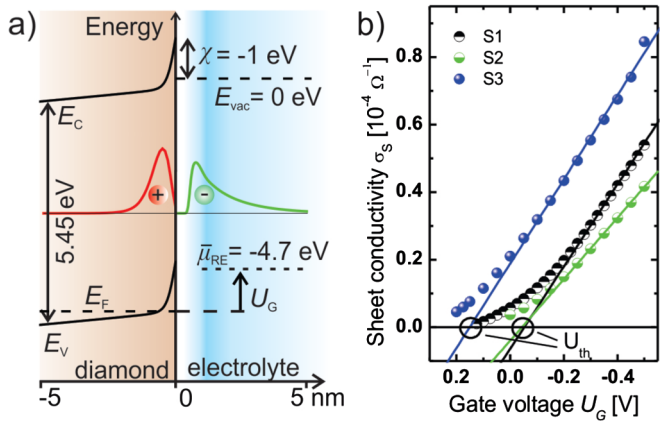

FIG. 1 (color online). (a) Simulated band diagram of the hydrogen-terminated diamond/electrolyte interface. The Fermi level E_F can be shifted below the valence band edge E_V at -4.45 eV with a gate potential U_G applied between the reference electrode $\bar{\mu}_{\mathrm{RE}}$ and a contact on the diamond. In the resulting potential well carriers accumulate in a two-dimensional hole gas (2-DHG), leading to band bending at the surface. The hole density is mirrored by a net negative ion density on the electrolyte side. (b) Sheet conductivity versus gate potential acquired from a four-contact resistance measurement using the van der Pauw configuration. See the text for details.

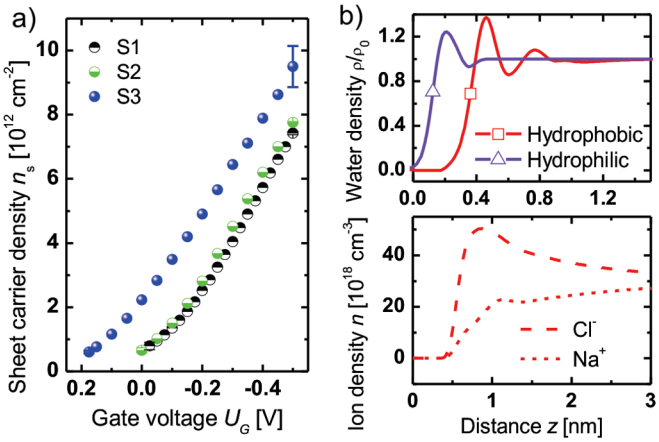

FIG. 2 (color online). (a) Sheet carrier density versus gate voltage, calculated from in-liquid Hall effect measurements. Above the threshold voltage, the three samples exhibit almost the same slope, which is determined by the interfacial capacitance. (b) Top: Water density profile at a hydrophobic and hydrophilic surface, as from molecular dynamics simulations [15]. Bottom: Ion density profile in the extended Poisson-Boltzmann model for 50 mM NaCl and a hole concentration of 5×10^{12} cm^{-2} in the diamond.

All samples investigated were (100)-oriented, single crystalline diamond (Diamond Detectors Ltd.) of optical grade, polished to a roughness of approximately 0.5 nm rms. Hydrogen termination of the diamond surface was achieved by using a microwave-generated hydrogen plasma (water contact angle approximately 85°) [5]. Conductivity and Hall effect measurements were performed in a van der Pauw configuration [3]. The samples were immersed in an electrolyte (10 mM potassium-based phosphate buffer and 50 mM NaCl) with the potential of the sample controlled by a potentiostat versus a Ag/AgCl reference electrode. Measurements were performed with lock-in amplifiers. The charge distribution and the electrostatic potential across the diamond/electrolyte interface were modeled with a Schrödinger-Poisson solver (nextnano^3 software) [12,13]. The single-band effective mass Schrödinger equations for heavy, light, and split-off holes in diamond are coupled to the overall Poisson equation via the charge density as described by the wave functions in the diamond and the ion density in the electrolyte. Both are solved numerically in one dimension and in an iterative and self-consistent manner, as has been previously described [13]. The Poisson equation is discretized on a nonuniform grid by using the finite differences method. For the electrostatic potential, we use the Dirichlet boundary condition $[\varphi(\infty) = U_G]$ in the bulk electrolyte and the Neumann boundary condition $[\partial\varphi/\partial x = 0]$ in the bulk diamond. The heavy and light hole bands are degenerate at the valence band maximum, and the split-off hole band is separated by 6 meV.

The surface conductivity was measured as a function of the applied gate voltage for different samples [Fig. 1(b)]. Conductivity values of 10^{-4} S as well as threshold voltages of 150 to -50 mV are in agreement with previously published results [5]. Above the threshold voltage U_{th}, the sheet conductivity σ_S increases approximately linearly with the applied gate potential U_G according to $\sigma_S = \mu C[-(U_G - U_{\mathrm{th}}) + \frac{1}{2}U_{\mathrm{DS}}]$, where μ is the field-effect mobility, C the interfacial capacitance, and U_{DS} the drain source voltage [10]. The difference in threshold voltage can be explained by residual oxygen termination or surface charges. An increase in the density of surface oxygen groups leads to a shift of the electron affinity towards more positive values, e.g., to $+1.7$ eV for a completely oxidized surface. This in turn changes the gate potential which is necessary to push the Fermi level below the valence band, thereby changing the onset of conductivity [see Fig. 1(a)]. The slope of the $\sigma_S(U_G)$ curve is proportional to the product of mobility μ and the diamond/electrolyte interfacial capacitance C.

The determination of the Hall voltage enables the characterization of the carrier concentration and, together with the conductivity data, the Hall mobility of the charge carriers. Above the threshold voltage, all samples show a nearly linear increase of the carrier concentration with the gate potential [Fig. 2(a)]. Together with the nearly linear increase of the conductivity [Fig. 1(b)], this results in the almost constant mobility with sample-dependent values between 30 and 70 cm^2/V s in the investigated range of carrier concentrations. The observed increase in the carrier concentration supports the model represented in Fig. 1(a). The slope of the carrier concentration versus gate potential

is almost the same for all samples, corresponding to a capacitance of the diamond/aqueous electrolyte interface of about 2 μF/cm^2. This is in agreement with results obtained by cyclic voltammetry and impedance spectroscopy [14].

In order to quantitatively understand the modulation of the carrier density in diamond with the electrolyte potential, we have to consider the charge distribution at the diamond/electrolyte interface in more detail. The applied gate voltage cannot be directly related to the electrostatic potential in diamond, since part of the applied voltage drops in the electrolyte close to the diamond surface. We model this interface by using the nextnano^3 software. In the diamond part, three single-band effective mass Schrödinger equations for the valence band edges (heavy hole, light hole, and split-off hole) are solved and coupled to the Poisson equation. The occupation of the subbands is determined by their position relative to the Fermi level. The electrolyte part of the interface is simulated by using a Poisson-Boltzmann model, which considers two different descriptions of the electrolyte. On the one hand, the electrolyte was modeled with a homogeneous dielectric constant of water by using the bulk value of $\epsilon_r = 78$; we term this the Poisson-Boltzmann (PB) model. On the other hand, a spatially varying dielectric constant $\epsilon_r(z)$ of water at the interface has been used, according to molecular dynamics simulations, which take the structure of water in the vicinity of a model hydrophobic surface into account [15]. These simulations yield a clear difference in the density of water close to a hydrophobic versus a hydrophilic surface, where at the former the depletion length is approximately 0.34 nm [Fig. 2(b)] [15]. We assume the dielectric constant to vary proportionally with the water density. Any effect of the ordering of water molecules [16] on the dielectric constant is assumed to be of second order compared to the influence of the hydrophobic gap and, thus, not considered. Furthermore, the Boltzmann distribution was modified to include a varying potential of mean force (PMF), describing the interaction between an ion and the hydrophobic interface for each of the ion species, according to the parametrization by Schwierz, Horinek, and Netz [15]. The PMFs result from molecular dynamics simulations of ions and their hydration shells in the vicinity of the surface [15]. They lead to an individual distribution for each of the ion species at the interface, depending on the hydrophobicity of the surface and the positive countercharge in the diamond [Fig. 2(b)]. The water density as well as the ion distribution vanishes close to a hydrophobic surface. Both contributions together constitute a model, which we refer to as extended Poisson-Boltzmann (ePB), and can be described by

$$\epsilon_0 \nabla_z [\epsilon(z) \nabla_z \varphi(z)] = -e \sum_i z_i n_i^0 \exp\left(-\frac{1}{k_B T}(V_i^{\mathrm{PMF}}(z) + \{z_i e[\varphi(z) - \varphi_l]\})\right),$$

where $\varphi(z)$ is the electrostatic potential, $\epsilon(z)$ the varying dielectric constant, $V_i^{\mathrm{PMF}}(z)$ the potential of mean force, φ_l the potential in the bulk electrolyte, z_i the valency, n_i^0 the nominal concentration of the ion i, and e the positive elementary charge. Figure 3(a) shows the potential $\varphi(z)$ across the diamond/electrolyte interface for both models, when a gate voltage of 0.3 V is applied. There is a striking difference in the potential drop in the electrolyte and, consequently, in the diamond for both models. As a result, the Fermi level is pushed further below the valence band edge for the PB model, in contrast to the ePB model.

The PB model allows an infinitely close approach of the ions to the interface as well as a high dielectric constant value for water close to the surface, thus minimizing the potential drop in the electrolyte. On the other hand, in the ePB model the depletion of water and ions in the direct vicinity of the surface induces a significant potential drop in the electrolyte. The correspondingly smaller potential drop in the diamond for the ePB model results in a lower concentration of charge carriers beneath the diamond surface. From the calculation of the carrier concentration at different applied potentials across the diamond/electrolyte interface, the interfacial capacitance for both models can be estimated. In Fig. 3(b), the U_G-dependent carrier

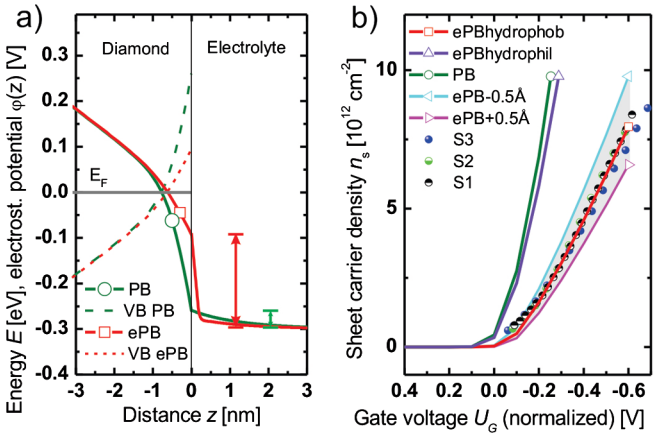

FIG. 3 (color online). (a) nextnano^3 simulations showing the potential drop across the diamond/electrolyte interface and the corresponding position of the valence band (VB) with respect to the Fermi level. (Only the region around the interface ± 3 nm is displayed; arrows indicate the potential drop in the electrolyte.) The PB model (olive) assumes the bulk properties of the electrolyte ($\epsilon_r = 78$) up to the interface. The ePB model (red) allows for a depletion of electrolyte in the vicinity of the hydrophobic surface. (b) Comparison between the simulated results [(a)] and the experimentally obtained carrier concentrations [Fig. 2(a)], for different gate potentials. All data sets are normalized with respect to their threshold voltage. The ePB for the hydrophobic interface, the conventional PB model, and the ePB model for a hydrophilic interface are compared. Results of the ePB model for the hydrophobic case, when a shift of the water density of ± 0.5 Å is considered, are additionally shown (cyan and magenta).

concentration revealed by the in-liquid Hall effect measurements is compared to the calculations for both models, after normalization with respect to the threshold voltage. The agreement between the extended Poisson-Boltzmann model and the slope of the experimental data is remarkable. We note that the calculations are based on a model hydrophobic surface. In order to assess the influence of the size of the water-depleted region, the water density profile has been shifted by ± 0.5 Å with respect to the surface (a typical variation for different hydrophobic surfaces). A similar shift of the PMFs has only a negligible influence on the results. The Poisson-Boltzmann model, also depicted in Fig. 3(b), clearly overestimates the capacitance of the diamond/electrolyte interface, as it does not take into account the depletion of ions and water at the hydrophobic interface. The importance of the hydrophobicity becomes even clearer when the extended Poisson-Boltzmann model is used with the parameters relevant for hydrophilic surfaces [Fig. 3(b)] [15], where ions and water can approach the surface much closer; the results resemble those of the PB model. The shortcomings of the PB model are less pronounced for hydrophilic surfaces such as the Si/SiO2/electrolyte interface, investigated in previous studies, e.g., [13].

This hydrophobic gap with a low water density in the vicinity of the diamond surface is in agreement with studies of other hydrophobic systems where a water density depletion has been observed [17–19].

The hole accumulation at the hydrogen-terminated diamond/aqueous electrolyte interface can therefore be simulated to great accuracy with the extended Poisson-Boltzmann model, showing the importance of explicitly accounting for the hydrophobic nature of surfaces. In this model the surface hydrophobicity limits the approach of the electrolyte ions to the surface and consequently increases the potential drop in the electrolyte, which reduces the effective potential at the semiconductor surface. As a result of the modification of the interfacial capacitance for hydrophobic surfaces, the sensitivity of potentiometric biosensor devices, which depends on the variation of the number of charge carriers with potential change, is profoundly affected. Accordingly, this effect is also relevant for other hydrophobic surfaces such as graphene, some self-assembled monolayers, and organic semiconductors [3,20]. Furthermore, other processes which require a close approach of, e.g., solvated molecules to the interface, such as charge transfer phenomena, e.g., in amperometric sensors or heterogeneous catalysis, can be affected by the hydrophobic gap.

The authors are grateful to N. Schwierz, D. Horinek, and R. Netz for helpful discussions regarding the potentials of mean force and the interfacial water depletion. This work was funded by the EU project DREAMS, FP6-NMP-2006-676033345, and by the Nanosystems Initiative Munich (NIM).

*garrido@wsi.tum.de

[1] C. E. Nebel *et al.*, J. Phys. D **40**, 6443 (2007).
[2] J. Kong *et al.*, Science **287**, 622 (2000).
[3] M. Dankerl *et al.*, Adv. Funct. Mater. **20**, 3117 (2010).
[4] W. S. Yang *et al.*, Nature Mater. **1**, 253 (2002).
[5] M. Dankerl *et al.*, Adv. Funct. Mater. **19**, 2915 (2009).
[6] D. Chandler, Nature (London) **437**, 640 (2005).
[7] M. I. Landstrass and K. V. Ravi, Appl. Phys. Lett. **55**, 975 (1989).
[8] F. Maier *et al.*, Phys. Rev. Lett. **85**, 3472 (2000).
[9] H. Kawarada *et al.*, Phys. Status Solidi A **185**, 79 (2001).
[10] A. Hartl *et al.*, J. Am. Chem. Soc. **129**, 1287 (2007).
[11] J. Ristein, W. Zhang, and L. Ley, Phys. Rev. E **78**, 041602 (2008).
[12] S. Birner *et al.*, IEEE Trans. Electron Devices **54**, 2137 (2007).
[13] S. Birner, C. Uhl, M. Bayer, and P. Vogl, J. Phys. Conf. Ser. **107**, 012002 (2008).
[14] J. A. Garrido, S. Nowy, A. Hartl, and M. Stutzmann, Langmuir **24**, 3897 (2008).
[15] N. Schwierz, D. Horinek, and R. R. Netz, Langmuir **26**, 7370 (2010).
[16] F. Sedlmeier *et al.*, Biointerphases **3**, FC23 (2008).
[17] J. J. Kuna *et al.*, Nature Mater. **8**, 837 (2009).
[18] M. Mezger *et al.*, Proc. Natl. Acad. Sci. U.S.A. **103**, 18 401 (2006).
[19] D. M. Huang *et al.*, Phys. Rev. Lett. **101**, 226101 (2008).
[20] M. E. Roberts *et al.*, Proc. Natl. Acad. Sci. U.S.A. **105**, 12 134 (2008).